ORIGINAL ARTICLE

Mechatronic stiffness of cable-driven mechanisms: a study on production machine model

Zdeněk Neusser[1] · Martin Nečas[1] · Jan Pelikán[1] · Jindřich Karlíček[1] · Vít Pawlik[1] · Petr Beneš[1] · Martin Machálka[2] · Zbyněk Šika[1] · Michael Valášek[1]

© The Author(s) 2022

Abstract

Position control of the mechanical structure with naturally limited stiffness is a common problem. Moreover, the system is usually exposed to random exciting by the external force effects and yet it is needed to hold the system in the desired position. Such an example in engineering practice can be the machine tool quill slim structure, which determines the machining accuracy and the machined surface quality. The limited structure stiffness can be overcome by suitable support structure solution. In principle, it is a matter of introducing the necessary force effect in the place where it is necessary to ensure the required position. A promising means how to apply control force to the flexible structure tip can be a thin cable structure with the force actuation and proper force control. The resulting system is characterized by increased stiffness achieved in a mechatronic manner. Therefore, the introduced concept is called mechatronic stiffness. The article describes selected mechanical arrangement of the mechatronic stiffness concept, its features, behaviour and control results. The proposed approach offers a solution for precise position control of the flexible structure. An experimental device was created in parallel with the simulation experiment and preliminary simulation results are obtained. The described concept is transferable to other flexible structures such as various manipulators.

1 Introduction

Modification of mechanical structure parameters is a non-trivial task. One of the crucial parameters is system eigenfrequencies, which are influenced by mass, moment of inertia, stiffness and damping of the system. The concept of the so-called mechatronic stiffness increases the structure properties by adding the auxiliary lightweight structure equipped with feasible control law. The auxiliary structure is in parallel with the basic structure interconnected by actuators. The concept of mechatronic stiffness is introduced with

the aim of the machine working point active control from zero frequency by means of the connection of the auxiliary structure, [1, 2]. The mechatronic stiffness gives greater possibilities than, for example, an active dynamic absorber, which affects the system from the certain oscillation frequency. On the other hand, compared to a dynamic absorber, mechatronic stiffness requires a design modification limiting the working space of the machine, which is a weakness compared to a dynamic absorber. In this paper, the concept of mechatronic stiffness is realized using cables, which significantly corrects this weakness of the concept. We therefore see a novelty in the cable realization of mechatronic stiffness. Such idea is presented, verification testbed is prepared and preliminary experimental results are obtained.

In areas, where structures undergo high force amplitudes or there is a demand for lightweight design, overall stiffness becomes significant property. Large machine tools suffer by large deflection during machining process. Reaching the desired stiffness of the machine often implies heavy structure. This leads to complications like large thermal effects,

✉ Zdeněk Neusser
zdenek.neusser@fs.cvut.cz

1 Department of Mechanics, Biomechanics and Mechatronics, Faculty of Mechanical Engineering, Czech Technical University in Prague, Technická 4, Prague 160 00, Czech Republic

2 TAJMAC-ZPS, a. s., třída 3. května 1180, Zlín 763 02, Czech Republic

high inertia and low chatter stability due to low eigenfrequencies [3]. Influence of large machine's compliance and inertia on its accuracy is analysed in [3]. Disturbance rejection algorithm based on measured acceleration of large machine tool is presented in [4]. The adaptation of control algorithm to improve a chatter stability which is influenced by dynamics of large tool is addressed in [5]. Variation of stiffness using piezoelectric actuators to reduce chatter during milling is presented in [6]. The improvement of static and dynamic behaviour of long slender tool holder by using pre-stressed segments and frictional damping is described in [7]. Active compensation of dynamic and static deformation of portal machine tool is presented in [8]. In [9], a nonlinear dynamic vibration absorber is used to combat vibrations of a boring bar, and vibration absorbers as delayed resonators could be used for ceasing simultaneously more frequencies [10, 11] and more dimensions too [12, 13].

Another approach is to increase the stiffness of whole system by optimization its mechanical structure. Paper [14] presents bio-inspired design of machine tools with increased stiffness. In [15], increase of stiffness of large column type machining tool through structural optimization was achieved. An overview of usage of composite materials in production machines is presented in [16]. Common serial robots are nowadays also used for machining. However, the lack of stiffness narrows the field of their application. Paper [17] treats the issue of low stiffness via optimization of workpiece position. A method for performance improvement of machining serial robots is proposed in [18]. Advanced controller for tool tip position adaptation during milling is designed in [19].

In lightweight mechanical systems, stiffness is also a challenging issue. Design concepts for lightweight structures are proposed in [20, 21]. Design of intelligent lightweight machine slides is described in [16]. Among the lightweight mechanical systems, the research of long slender compliant structures, e.g. manipulators, is popular in present. A cable-driven segmented manipulator with improved linkage mechanism for securing high stiffness and accuracy is presented in [22]. The dynamic properties of a cable-beam system with cantilever beam and the wires connected to its tip have been explored with wires being perpendicular in [23] and parallel [24]. A flexible manipulator with two cables is studied in [25]. Holland et al. [26] deals with vibration of a tapered cantilever beam with a wire connected to its tip. The wires, in combination with a control strategy, can be used to suppress vibrations of the beam, such as in [27]. To be able to transfer force through a cable, the dynamical properties of the cable must be also known and included in the control. The behaviour of a fibre has been modelled with respect to fibre mass, stiffness and damping [28–31]. In [32], stiffness of cables with large strains has been studied. A 10-m-long

articulated tendon-driven manipulator designed for Fukushima power plant investigation is described in [33]. Modelling and control of slender tendon-driven manipulators are discussed in [34, 35]. In some areas like physical human robot interaction or collaborative robotics, the ability to vary stiffness during operation could be advantageous. Promising in this field is the research of variable stiffness/impedance actuators, which utilizes their intrinsic compliance [36]. The benefits concern e.g. agile motions [37], safety [38], energy efficiency [37, 39] or soft object handling [40].

The important part of the mechatronic stiffness concept is control algorithm. Using existing actuators with a new control strategy allows vibration suppression [41] and could be used for stiffening the feedback. Another control solution is proposed in [42] combining input shaping with the addition of servo control. In [43], the prediction of the position error is used to modify the input command of a dual-driving gantry-type machine to improve accuracy. In [44] a control strategy is designed to reduce vibrations of the tip of a long and flexible manipulator. The underactuated mechanical systems residual vibration cancelation is investigated in [45, 46]. The machine redundancy is investigated in [47] and control with sliding mode control is presented in [48]. Parallel manipulator modeling and vibration analysis [49] and electro-mechanical performance prediction using similitude analysis are performed in [50]. Feedforward control of industrial hybrid robot improves accuracy using iterative learning method in [51].

To explore the dynamics of manufacturing machines, nonlinear models are used to model contacts in ball screw [52], vibration of guideways [53], drive mechanisms [54] and in modelling the cutting vibrations resulting from tool-workpiece interaction [55, 56]. The micro-manufacturing technology is presented in [57]. Multi-scale modelling and analysis of high-precision aerostatic bearing slideway is shown in [58].

In this study, the mechanical properties improvement of production machine working point (TCP) using auxiliary cable structure is presented. A concept of the so-called mechatronic stiffness is presented in [1, 2]. The novelty extending the concept is based on adding cables driven by standard rotary drives, which create the auxiliary parallel structure and bring additional force near to the machine working point (TCP). The cable structure application in combination with the machine tool positioning task is a novel topic. According to the best knowledge of the authors, the investigation of the presented machine tool cable-based mechatronic stiffness is so far very limited. The simplified model of machine tool construction is used, the model is prepared and the control using computed torques with PD controller is assembled. The frequency analysis and simulation experiment are provided as well as preliminary experimental results.

The paper is organized as follows. In the first section, the motivation and literature survey is prepared, and the second section shows the experimental setup model and its parameters identification. The third section is dedicated to the feasible control law design and the fourth section shows the simulation experiment results. The next section presents the preliminary experimental results and the last section concludes the work.

2 Model of experimental stand

Physical model of experimental setup is presented in this section. A simple experimental demonstrator is assembled for the investigation of a mechatronic stiffness concept. The stand is shown in Fig. 1 and is designed in order to include main dynamic properties of machine tools with a large workspace and long heavy movable parts. The details of system identification and equations derivation are in [59].
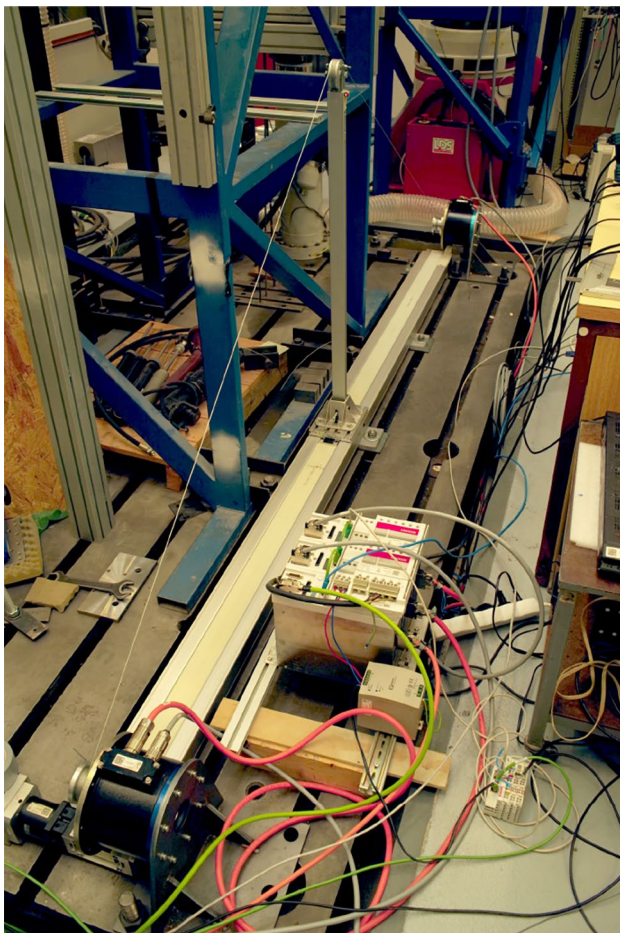

Fig. 1 Experimental stand with equipment

A simplified multibody simulation model is created, based on the exprimental stand. The model coordinates and parameters are shown in Fig. 2. The electric servo drives have inputs i_i and outputs are torques M_i. The cart movement is prescribed as separate input. Cable mass is neglected. The equations of motion are assembled using a free body diagram method. All force effects and particular body coordinates are depicted in Fig. 3. Equations of motion resulting from Fig. 3 are

$$
\begin{aligned}
I_1 \ddot{\varphi}_1 &= M_1 - F_1 r_1 - b_{M1} \dot{\varphi}_1 \\
I_2 \ddot{\varphi}_2 &= M_2 + F_2 r_2 - b_{M2} \dot{\varphi}_2 \\
m \ddot{x}_n &= -F + F_2 \cos \alpha_2 - F_1 \cos \alpha_1
\end{aligned}
\tag{1}
$$

where φ_1, φ_2 coordinates are angular positions of electric servo drive rotors, x_n is horizontal coordinate of the TCP and x represents horizontal cart position.

The equations of motion (1) include inertial forces, force of beam elasticity, cable forces, damping forces characterised by damping coefficients b_{M1}, b_{M2} and cable angles α_i. Forces F, F_1 and F_2 are expressed as

$$
\begin{aligned}
F_1 &= \frac{k_1}{L_1} \xi_1 + \frac{b_1}{L_1} \dot{\xi}_1 \\
F_2 &= \frac{k_2}{L_2} \xi_2 + \frac{b_2}{L_2} \dot{\xi}_2 \\
F &= k(x_n - x) + b(\dot{x}_n - \dot{x})
\end{aligned}
\tag{2}
$$

Extensions ξ_i of cables are evaluated in (3). They are based on Fig. 4. The left part of the figure depicts the angle α_i derivation, it is measured from the x axis, and the right part shows cable length including segments wound on pulleys. Both cables properties are presumed to be the same. Stiffness equals to k_L, $k_1 = k_2 = k_L$, damping equals to b_L, $b_1 = b_2 = b_L$. Stiffness and damping are in reciprocal proportion to the length of the cable.

Cable longitudinal deformation (cable extension) equals to difference of actual cable length and initial cable length:

$$
\begin{aligned}
\xi_1 &= L_1 - L_{10} + (r - r_1)(\alpha_1 - \alpha_{10}) + \varphi_1 r_1 \\
\xi_2 &= L_2 - L_{20} + (r - r_2)(\alpha_2 - \alpha_{20}) - \varphi_2 r_2
\end{aligned}
\tag{3}
$$

where symbols L_{10}, L_{20} and α_{10}, α_{20} correspond to initial cable lengths and cable angles, respectively. Actual cable lengths and angles are derived from Fig. 4 as

$$
\begin{aligned}
L_1 &= \sqrt{(x_n + \Delta x_1)^2 + (y_n - y_1)^2 - (r_1 - r)^2} \\
L_2 &= \sqrt{(\Delta x_2 - x_n)^2 + (y_n - y_2)^2 - (r_2 - r)^2} \\
\alpha_1 &= \beta + \gamma = \arctan\left(\frac{y_n - y_1}{x_n + \Delta x_1}\right) + \arctan\left(\frac{r_1 - r}{L_1}\right) \\
\alpha_2 &= \arctan\left(\frac{y_n - y_2}{\Delta x_2 - x_n}\right) + \arctan\left(\frac{r_2 - r}{L_2}\right)
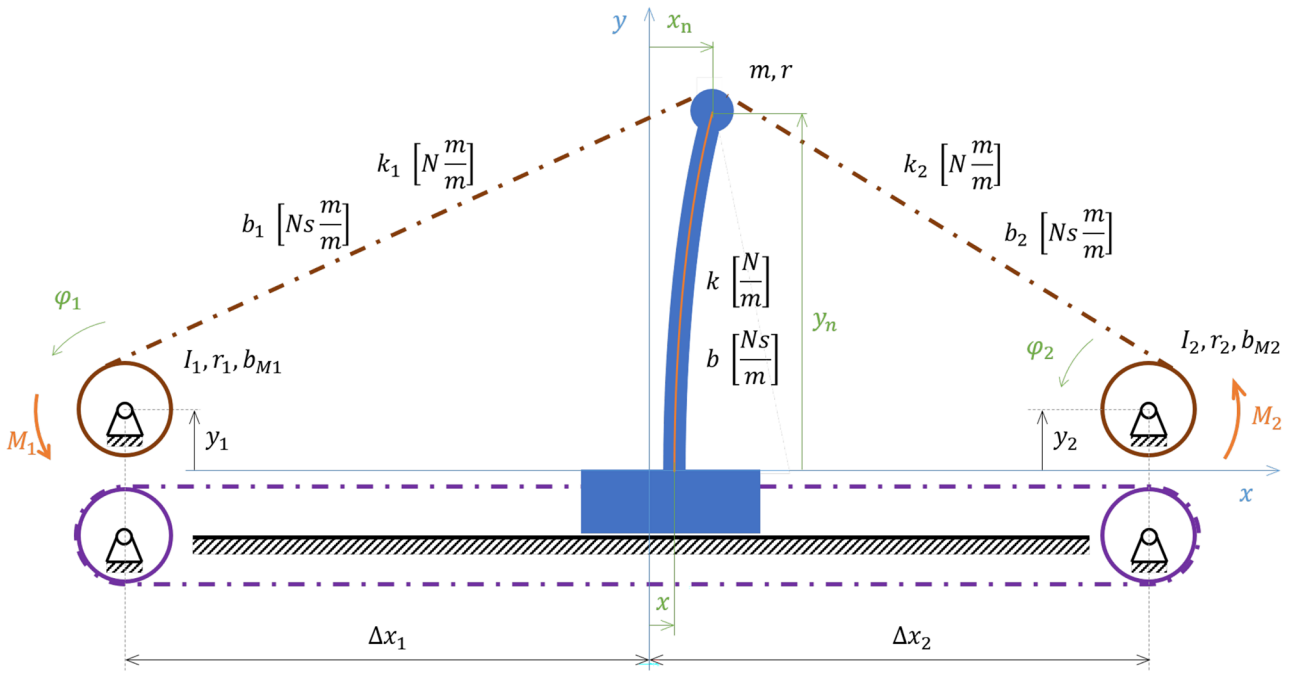\end{aligned}
\tag{4}
$$

Fig. 2 Mechanical model of the experimental stand with coordinate system (blue), coordinates (green) and parameters (black). The additional auxiliary structure is in brown

with the only time dependent variable x_n, the rest of the parameters are constants. Radii r_1 and r_2 are first and second motor cable pulleys, and r is the beam tip cable pulley radius. The beam deformation is assumed to be small; therefore, the beam tip coordinate y_n does not change its value.

Cable extension velocities $\dot{\xi}_1$ and $\dot{\xi}_2$ used in (2) are time derivative of Eq. (3) and time derivative of particular members of (4):

$$\dot{\xi}_1 = \dot{L}_1 + (r - r_1)\dot{\alpha}_1 + \dot{\varphi}_1 r_1$$
$$\dot{\xi}_2 = \dot{L}_2 + (r - r_2)\dot{\alpha}_2 - \dot{\varphi}_2 r_2 \qquad (5)$$
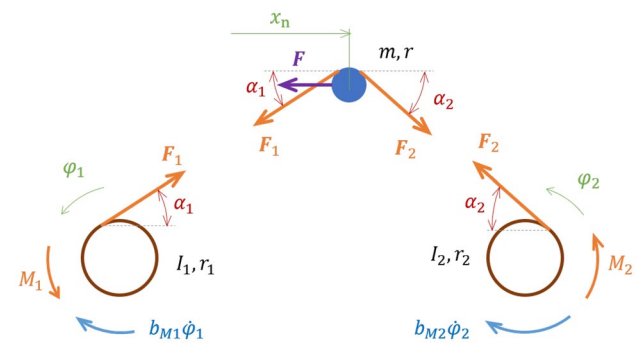

Fig. 3 Free body diagram. The beam is simplified as horizontally moving mass, the cart is kinematically actuated, that is why it is not taken into account

The electromagnetic field in the BLDC drive produces the rotor torque M_1 and M_2. The torque is modelled as proportional to the stator armature current:

$$M_1 = k_{t1} i_1$$
$$M_2 = k_{t2} i_2 \qquad (6)$$

with the current constants k_{t1} and k_{t2} of the first and second motor.

The moments of inertia I_1, I_2, the equivalent beam mass m, damping coefficients b_{M1}, b_{M2} from the equations of motion (1), stiffnesses k, k_L, damping coefficients b, b_L from the forces Eq. (2) and parameters k_{t1}, k_{t2} from (6) are subject of identification process while being unknown.

2.1 System parameters identification

Model parameters are assessed in this sub-section. The important property of all parameters lies in the linearity. They create a system of linear equations (mostly time dependent). Due to the measurement of other system parameters than just inputs and output, the identification process is separated into three parts: beam identification, cable properties identification and electric drive 1, electric drive 2 identification.

Fig. 4 Sketch for derivation of cable angle (left) and cable length (right)
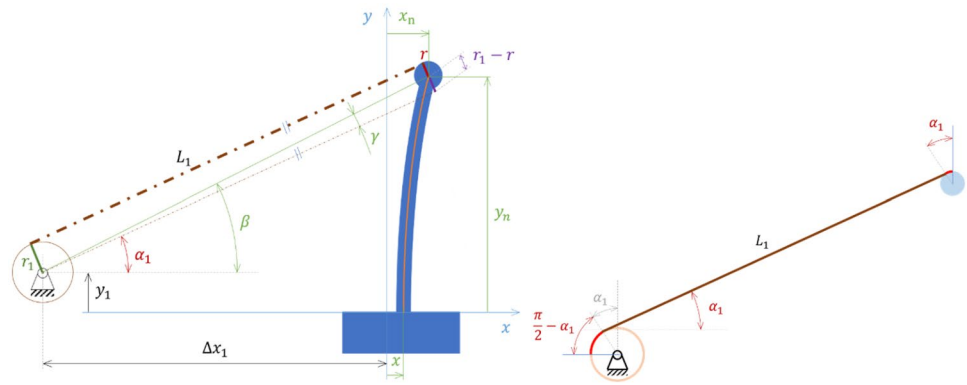
The beam properties are obtained from the experiment, where the deflected beam is released and its movement gives the damped vibratory behaviour as an identification input. Identification of cable and drive parameters is performed using experiment with sweep cosine signal as an input at drives subsequently. The constant cable pre-load is ensured by the other drive. The excitation frequency range is from the $0.5Hz$ up to $30Hz$, which is a reasonable range for exciting the first eigenfrequencies. The beam end-point horizontal position and drive angular positions are measured. Data acquisition and further processing keeps the measurement sampling frequency $f_s = 1kHz$.

2.1.1 Beam properties

The cart has an attached fixed beam, which is modelled as a cantilever. The first eigenmode causes the beam dominant vibrations. The beam deflection analytical solution and experimental data give the basis for k, b, m identification.

Figure 5 presents the experiment of fixed cart and initially deflected beam free oscillations measured by KISTLER accelerometer type 8312B10. Two oscillation periods (left part of

the figure) of the beam are measured and damped system eigenfrequency is obtained, $f_{beam_d} = 10.8108\ Hz$.

Damping ratio is obtained from Fig. 5, right. The ration between oscillation amplitudes at the beginning and after some time gives us damping ration $\zeta = 4.635 \cdot 10^{-3}$ and undamped eigenfrequency (further just eigenfrequency) $f_{beam} = 10.8109\ Hz$.

Obtained parameters (damping ratio and eigenfrequency) do not uniquely give the k, b and m parameters of the reduced beam model. The fixed beam horizontal deflection equation allows beam horizontal stiffness calculation at beam reduced mass position. Beam length $L = 0.95m$, material young modulus $E = 70 \cdot 10^9 Pa$ and cross-section quadratic moment $J = 1.88 \cdot 10^{-8} m^4$ are inputs for beam stiffness evaluation:

$$k = \frac{3EJ}{L^3} = 4604.75 \frac{N}{m} \tag{7}$$

Using the homogeneous part of the third equation of motion from (1) with substituted force F from (2), beam equivalent mass m and beam damping b are derived:

Fig. 5 Beam parameters identification, oscilloscope screenshots

$$m = \frac{k}{(2\pi f_{beam})^2} = 0.998 kg$$

$$b = 2\zeta(2\pi f_{beam})m = 0.63\frac{Ns}{m} \tag{8}$$

2.1.2 Cable properties

The experimental stand at Fig. 1 is equipped with light-weight wound metallic cable with characteristic stiffness k_L and damping b_L. The cable has the same properties on both sides of the experimental setup. The identification of cable properties is performed using experimental measurement. The experiment is the following: sweep cosine load is introduced at drive one (on the left) and constant load serving as necessary cable pre-stress is applied at drive two (on the right).

The third equation of motion from (1) is used for the identification analysis. Substituting the forces (2) into this equation, it is obtained:

$$m\ddot{x}_n + b(\dot{x}_n - \dot{x}) + k(x_n - x)$$
$$= k_L\left(\frac{\xi_2}{L_2}\cos\alpha_2 - \frac{\xi_1}{L_1}\cos\alpha_1\right) + b_L\left(\frac{\dot{\xi}_2}{L_2}\cos\alpha_2 - \frac{\dot{\xi}_1}{L_1}\cos\alpha_1\right) \tag{9}$$

where unknown parameters k_L and b_L are in linear combination. Other parameters and terms are known or could be derived from the measured data and its numeric time derivative. Numeric time derivative is amended with non-causal zero-phase low pass data filtering.

Stiffness $k_L = 16432\frac{Nm}{m}$ and damping $b_L = 131\frac{Nms}{m}$ are obtained using least-square method. Resulting values are verified in the simulation experiment, where the Eq. (9) has angles φ_1, φ_2 and cart position x as inputs. The comparison of model simulation and experimental behaviour in frequency domain is in Fig. 6. The frequency content is similar, and the magnitudes slightly differ.

2.1.3 Electric drives properties

The electric drives parameters identification is founded on the similar experiment as in Sect. 2.1.2. Rotor moments of inertia I_1, I_2, bearing dampings b_{M1}, b_{M2} and current constants k_{t1}, k_{t2} from (6) are parameters of drives according to Fig. 2. The inputs (winding currents i_1 and i_2), rotor angular positions φ_1, φ_2 and the horizontal position of beam tip point x_n are recorded.

The first and the second equations of motion from the (1) are taken into account for the identification analysis.

Fig. 6 Verification of identified model: cable parameters, frequency analysis. Comparison between measurement and simulation using measured inputs and identified system parameters
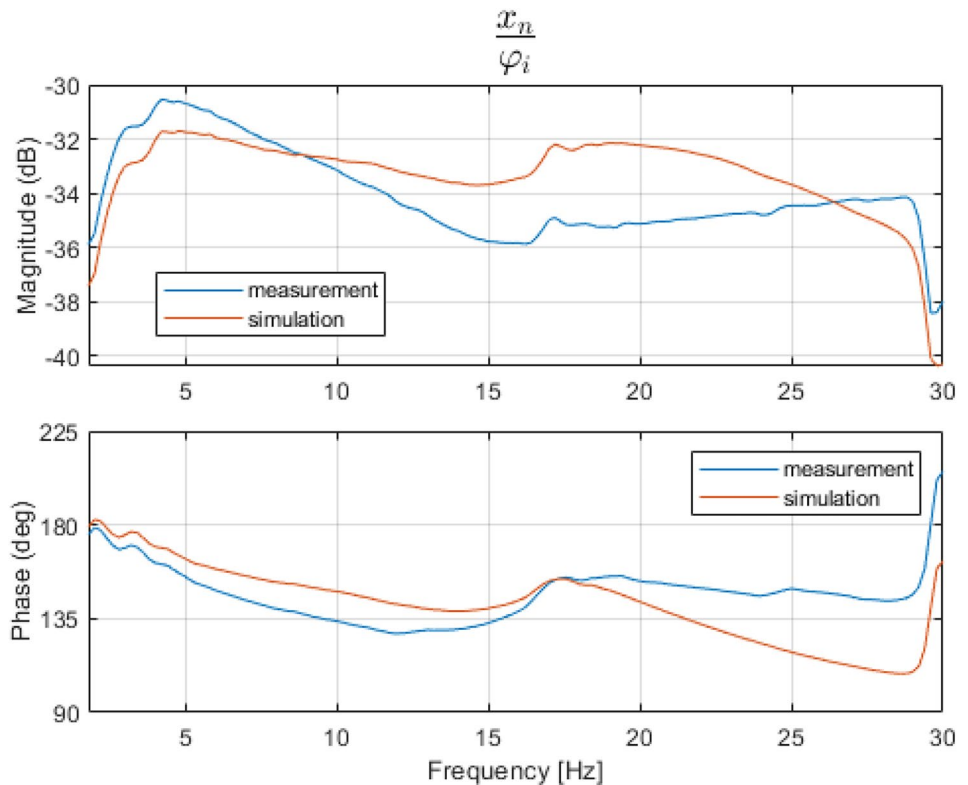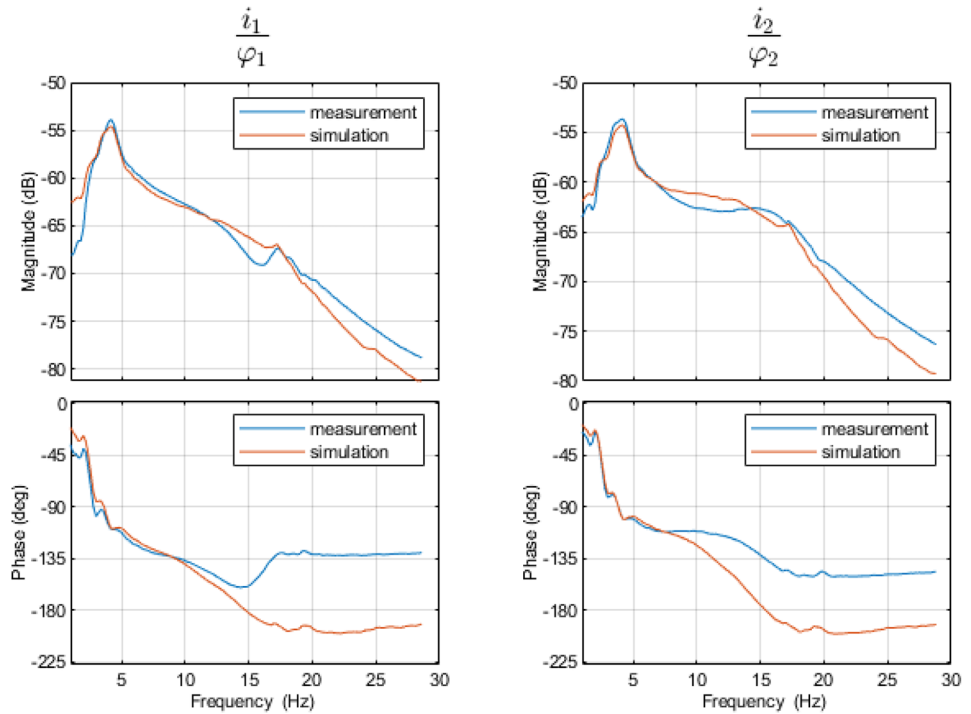
Fig. 7 Verification of identified model: drive parameters, frequency analysis. Comparison between measurement and simulation using measured inputs and identified system parameters for both drives

Introducing the forces (2) and electromagnetic moments (6) into those particular equations, it is obtained:

$$\left(\frac{k_L}{L_1}\xi_1 + \frac{b_L}{L_1}\dot{\xi}_1\right)r_1 = k_{t1}i_1 - I_1\ddot{\varphi}_1 - b_{M1}\dot{\varphi}_1$$
$$-\left(\frac{k_L}{L_2}\xi_2 + \frac{b_L}{L_2}\dot{\xi}_2\right)r_2 = k_{t2}i_2 - I_2\ddot{\varphi}_2 - b_{M2}\dot{\varphi}_2 \tag{10}$$

where unknown parameters $k_{t1,2}$, $I_{1,2}$ and $b_{M1,2}$ are in the linear combination. Other parameters and terms are known or could be derived from the measured data and its numeric time derivative. Numeric time derivative is amended with non-causal zero-phase low pass data filtering as in the previous case.

Moments of inertia $I_1 = 7.98 \cdot 10^{-4} kgm^2$, $I_2 = 8.74 \cdot 10^{-4} kgm^2$ $I_2 = 8.74 \cdot 10^{-4} kgm^2$, current constants $k_{t1} = 0.15\frac{Nm}{A}$, $k_{t2} = 0.2\frac{Nm}{A}$ and dampings $b_{M1} = 0.035 Nms$, $b_{M2} = 0.005 Nms$ are obtained using the least-square method, similarly as in the previous case. Resulting values are verified in the simulation experiment, where Eq. (10) has currents i_1, i_2 and beam TCP position x_n as inputs. The comparison in frequency domain is at Fig. 7. The left part shows behaviour of the first motor, and the right part shows the behaviour of the second motor.

3 Motion control

The system at (1) has prescribed end-point (TCP) motion. The corresponding coordinate is x_n, with desired motion behaviour x_{nd}. The desired motion time derivatives are also given. The task is to move the system end point along the desired trajectory, i.e. trajectory tracking problem must be solved. The cables must be pre-stressed.

For the prescribed task, the computed-torque method with PD controller is chosen. The cable pre-load is also treated. In the following sub-section, computed-torque control is presented.

3.1 Computed-torque control with PD controller

The system dynamics is assumed to be described in the following form:

$$\mathbf{M}(\mathbf{q}, \dot{\mathbf{q}})\ddot{\mathbf{q}} = \mathbf{N}(\mathbf{q}, \dot{\mathbf{q}}) + \boldsymbol{\tau} \tag{11}$$

where $\mathbf{q}$ are system coordinates, $\mathbf{M}$ is inertia matrix, $\mathbf{N}$ contains external forces and $\boldsymbol{\tau}$ are system inputs. The coordinates acceleration $\ddot{\mathbf{q}}$ is derived

$$\ddot{\mathbf{q}} = \mathbf{M}(\mathbf{q}, \dot{\mathbf{q}})^{-1}(\mathbf{N}(\mathbf{q}, \dot{\mathbf{q}}) + \boldsymbol{\tau}) \tag{12}$$

The tracking error is defined as

$$\mathbf{e} = \mathbf{q}_d - \mathbf{q} \tag{13}$$

and differentiating it twice it is obtained

$$\ddot{\mathbf{e}} = \ddot{\mathbf{q}}_d - \ddot{\mathbf{q}} \tag{14}$$

where $\mathbf{q}_d$ are desired states behaviour. Substitution of (12) into (14) results in

$$\ddot{\mathbf{e}} = \ddot{\mathbf{q}}_d - \mathbf{M}(\mathbf{q}, \dot{\mathbf{q}})^{-1}(\mathbf{N}(\mathbf{q}, \dot{\mathbf{q}}) + \boldsymbol{\tau}) \tag{15}$$

The feedback linearization technique is used and new input variables **u** are defined:

$$\mathbf{u} = \ddot{\mathbf{q}}_d - \mathbf{M}(\mathbf{q}, \dot{\mathbf{q}})^{-1}(\mathbf{N}(\mathbf{q}, \dot{\mathbf{q}}) + \boldsymbol{\tau}) \tag{16}$$

and system (15) transforms into

$$\ddot{\mathbf{e}} = \mathbf{u} \tag{17}$$

To stabilize tracking error dynamics, the appropriate input variables **u** are chosen. The simple case is using a proportional-derivative (PD) controller (actually state-feedback of (17)) in the following way:

$$\mathbf{u} = -K_p \mathbf{e} - K_d \dot{\mathbf{e}} \tag{18}$$

The coefficients K_p and K_d are determined using pole placement methods (to ensure stability and robustness). The system inputs are derived using substitution of (18) into (16):

$$\boldsymbol{\tau} = \mathbf{M}(\mathbf{q}, \dot{\mathbf{q}})(\ddot{\mathbf{q}}_d + K_p \mathbf{e} + K_d \dot{\mathbf{e}}) - \mathbf{N}(\mathbf{q}, \dot{\mathbf{q}}) \tag{19}$$

3.2 Control of experimental stand: cart position and cable pre-load

The system (1) has three inputs: cart position x and stator armature currents i_1 and i_2. The system output is position of tool centre point with prescribed motion x_{nd}. With regard to the system design, the cart position and TCP position must have the same x-coordinate.

$$x = x_{nd} \tag{20}$$

Utilizing cables, the cable pre-load must exist to prevent the cables unload. Due to the structure of Eq. (20), the pre-tension is distributed on both sides. The right side (input i_2) is selected for cable pre-loading.

The force in the right cable is expressed

$$F_2 = \frac{k_L}{L_2}\xi_2 + \frac{b_L}{L_2}\dot{\xi}_2 \tag{21}$$

with prescribed F_{2d} as a cable pre-load force. Substituting the (3) and (5) into (21), it is obtained

$$F_2 = \frac{k_L}{L_2}\left(L_2 - L_{20} + (r - r_2)(\alpha_2 - \alpha_{20}) - \varphi_2 r_2\right) \\ + \frac{b_L}{L_2}\left(\dot{L}_2 + (r - r_2)\dot{\alpha}_2 - \dot{\varphi}_2 r_2\right) \tag{22}$$

Using (22) as a desired variable basis for the second eigenequation of motion (1), the φ_2 behaviour must be known. The angle φ_2 is derived from (22)

$$\varphi_2 = \frac{k_L\left(L_2 - L_{20} + (r - r_2)(\alpha_2 - \alpha_{20})\right) + b_L\left(\dot{L}_2 + (r - r_2)\dot{\alpha}_2\right) - F_2 L_2}{r_2(b_L s + k_L)} \tag{23}$$

Substituting the F_{2d} into the (23), the variable φ_{2d} is obtained. Their time derivatives are needed for the second eigenequation of motion (1).

$$\dot{\varphi}_{2d} = \frac{k_L\left(L_2 - L_{20} + (r - r_2)(\alpha_2 - \alpha_{20})\right) + b_L\left(\dot{L}_2 + (r - r_2)\dot{\alpha}_2\right) - F_{2d} L_2}{r_2 b_L} \\ - \varphi_{2d}\frac{k_L}{b_L} \tag{24}$$

$$\ddot{\varphi}_{2d} = \frac{k_L\left(\dot{L}_2 + (r - r_2)\dot{\alpha}_2\right) + b_L\left(\ddot{L}_2 + (r - r_2)\ddot{\alpha}_2\right) - F_{2d}\dot{L}_2}{r_2 b_L} - \dot{\varphi}_{2d}\frac{k_L}{b_L} \tag{25}$$

The second equation of (1) is used for computed torques method: the tracking error is according to (15)

$$e_1 = \varphi_{2d} - \varphi_2 \tag{26}$$

and feedback linearization is performed with new control variable u_1

$$\ddot{e}_1 = \ddot{\varphi}_{2d} - \ddot{\varphi}_2 = \ddot{\varphi}_{2d} - \frac{F_2 r_2 - b_{M2}\dot{\varphi}_2 + k_{t2} i_2}{I_2} = u_1 \tag{27}$$

The control law for u_1 is expressed according to (18)

$$u_1 = -K_{p1}\left(\varphi_{2d} - \varphi_2\right) - K_{d1}\left(\dot{\varphi}_{2d} - \dot{\varphi}_2\right) \tag{28}$$

and input variable i_2 is evaluated:

$$i_2 = \frac{I_2\left(\ddot{\varphi}_{2d} + K_{p1}\left(\varphi_{2d} - \varphi_2\right) + K_{d1}\left(\dot{\varphi}_{2d} - \dot{\varphi}_2\right)\right)}{k_{t2}} \\ + \frac{b_{M2}\dot{\varphi}_2 - F_2 r_2}{k_{t2}} \tag{29}$$

The input variable from (29) using appropriate feedback gains K_{p1} and K_{d1} ensures the constant pre-load of the cables.

3.3 Control of experimental stand: end point trajectory tracking

Mechanism end point trajectory tracking is ensured by the input i_1 (stator armature current of the first motor) using computed torques PD control in the cascade.

At first, the third eigenequation of motion from (1) is used to determine φ_{1d}, $\dot{\varphi}_{1d}$ and $\ddot{\varphi}_{1d}$ — desired motion of φ_1 coordinate and its time derivatives.

The second control loop is for the first equation from (1), which is a dynamic equation of the first motor, covering the

electromagnetic effects. The desired motion of φ_1 coordinate serves for determination of stator armature current i_1 as an overall system input.

3.3.1 Desired motion of φ_1 and its time derivatives

The third equation of motion from (1) is adapted in the following way

$$\ddot{x}_n = \frac{F_2 \cos \alpha_2 - F}{m} - \frac{\cos \alpha_1}{mL_1} \left(k_L \chi_1 + k_L r_1 \varphi_1 + b_L \dot{\chi}_1 + b_L r_1 \dot{\varphi}_1 \right) \tag{30}$$

where

$$\chi_1 = L_1 - L_{10} + \left(r - r_1 \right) \left(\alpha_1 - \alpha_{10} \right)$$
$$\dot{\chi}_1 = \dot{L}_1 + \left(r - r_1 \right) \dot{\alpha}_1$$

has initial cable length L_{10} and initial cable angle α_{10}. The tracking error is according to (13)

$$e_2 = x_{nd} - x_n \tag{31}$$

where x_{nd} is desired TCP x-coordinate motion. Using feedback linearization, the new input variable u_2 is defined

$$\ddot{e}_2 = \ddot{x}_{nd} - \ddot{x}_n = u_2 \tag{32}$$

According to (18), the control law for u_2 is set

$$u_2 = -K_{p2} \left(x_{nd} - x_n \right) - K_{d2} \left(\dot{x}_{nd} - \dot{x}_n \right) \tag{33}$$

and motor angle φ_1 behaviour is evaluated:

$$\varphi_1 = \left[\frac{L_1 \left(F_2 \cos \alpha_2 - F - m \left(\ddot{x}_{nd} - u_2 \right) \right)}{r_1 \cos \alpha_1} + \frac{k_L \chi_1 + b_L \dot{\chi}_1}{r_1} \right] \frac{1}{b_L s + k_L} \tag{34}$$

The appropriate angular velocity $\dot{\varphi}_1$ is

$$\dot{\varphi}_1 = \left[\frac{L_1 \left(F_2 \cos \alpha_2 - F - m \left(\ddot{x}_{nd} - u_2 \right) \right)}{r_1 \cos \alpha_1} + \frac{k_L \chi_1 + b_L \dot{\chi}_1}{r_1} - k_L \varphi_1 \right] \frac{1}{b_L} \tag{35}$$

and for the further progress the angular acceleration $\ddot{\varphi}_1$ is needed. Time derivative of the third equation (1) facilitates the expression for the angular acceleration.

The obtained φ_1, $\dot{\varphi}_1$ and $\ddot{\varphi}_1$ variables as φ_{1d}, $\dot{\varphi}_{1d}$ and $\ddot{\varphi}_{1d}$ are input for the next step of mechanism control procedure.

3.3.2 System input i_1 evaluation

The first drive desired motion $\ddot{\varphi}_{1d}$ is obtained in the previous section. Its equation of motion represents the first equation in (1). The angular acceleration is obtained in the following expression.

$$\ddot{\varphi}_1 = \frac{i_1 k_{t1} - F_1 r_1 - b_{M1} \dot{\varphi}_1}{I_1} \tag{36}$$

The corresponding tracking error is according to (13) following.

$$e_3 = \varphi_{1d} - \varphi_1 \tag{37}$$

The feedback linearization (according to (17)) on tracking error is

$$\ddot{e}_3 = \ddot{\varphi}_{1d} - \frac{i_1 k_{t1} - F_1 r_1 - b_{M1} \dot{\varphi}_1}{I_1} = u_3 \tag{38}$$

where new input variable u_3 is according to (18) PD controller on the tracking error coordinate e_3

$$u_3 = -K_{p3} \left(\varphi_{1d} - \varphi_1 \right) - K_{d3} \left(\dot{\varphi}_{1d} - \dot{\varphi}_1 \right) \tag{39}$$

and input variable i_1 is evaluated using (38) and (39):

$$i_1 = \frac{I_1 \left[\ddot{\varphi}_{1d} + K_{p3} \left(\varphi_{1d} - \varphi_1 \right) + K_{d3} \left(\dot{\varphi}_{1d} - \dot{\varphi}_1 \right) \right] + b_{M2} \dot{\varphi}_1 + F_1 r_1}{k_{t1}} \tag{40}$$

4 Simulation experiment: trajectory tracking

The simulation experiment for the presented mechanical system is performed. For obtaining of all system states, the state observer with measured inputs φ_1, φ_2 and x_n is used. There are two drive control strategies. The first is with drives in position control mode, and the second uses drives in torque control mode. For both cases, the control algorithm is assembled. Sensitivity on idenfied parameters inaccuracy was tested. With the 10% parameter deviation, the control works and results are close to the simulation without parameter deviation.

The PD controller parameters (K_{pi}, K_{di}, $i = 1, ..., 3$) are selected for the system derived from (17) and (18):

$$\ddot{\mathbf{e}} + K_{di} \dot{\mathbf{e}} + K_{pi} \mathbf{e} = 0 \tag{41}$$

where the proportional (K_{pi}) and derivative (K_{di}) coefficients are derived from the desired system roots for the ith controller. Roots are characterized by eigenfrequency Ω_i and damping ratio ζ_i.

The first controller (controls desired F_{2d} force in the cable) has $\Omega_1 = 30\frac{rad}{s}$ and $\zeta_1 = 0.7$; the second controller (transfers desired motion from TCP desired position to φ_1 coordinate) has frequency two times higher ($\Omega_2 = 60\frac{rad}{s}$) and $\zeta_2 = 0.5$. The last controller (ensures the φ_1 desired coordinate behaviour by the drive input i_1) is in cascade with previous controllers and frequency is three times higher than with second controller ($\Omega_3 = 180\frac{rad}{s}$ and $\zeta_3 = 0.7$). The state observer has eigenfrequencies $378\frac{rad}{s}$, $454\frac{rad}{s}$, $529\frac{rad}{s}$ and common damping 0.5. The damping is critical to facilitate the convergence, and the frequency is high enough to secure the sufficient controller bandwith.

The relations between damping, frequency and controller parameters are

$$K_{pi} = \Omega_i^2$$
$$K_{di} = 2\zeta_i\Omega_i \tag{42}$$

At the first, the simulated frequency response is obtained, and at the second, the trajectory tracking error is analysed during the prescribed motion.

4.1 Effect of cables with drives in position control mode

The system with the cables and drives in position control mode is at Fig. 8. It uses only part of the derived computed torques control equations. The cable pre-load force F_{2d} is substituted into the (23) and desired angular position φ_2 is obtained. The angular velocity $\dot{\varphi}_2$ is evaluated using (24). These are inputs of the right engine.

Follows the end point trajectory tracking task. The angle φ_1 is then evaluated using (34) with PD control law (33). The control law is extended with I part (43) to remove the residual control error, the I part gain K_I equals 10^4.

$$\ddot{\mathbf{e}} + K_{d2}\dot{\mathbf{e}} + K_{p2}\mathbf{e} + K_I \int \mathbf{e} = 0 \tag{43}$$

The angular velocity $\dot{\varphi}_1$ is then evaluated using (35). These are inputs of the left engine. The third equation of (1) is resulting system eigen equation of motion with inputs x, $\dot{x}$, φ_1, $\dot{\varphi}_1$, φ_2, $\dot{\varphi}_2$.

4.1.1 Frequency response

The frequency response of the nonlinear system is obtained by system excitation with harmonic signal. Follows the FFT signal analysis for obtaining transfer function of the system. The prescribed motion of TCP point (coordinate x_n) is used. The excitation input signal is harmonic chirp with frequency range from 0.1 to 50Hz. The amplitude of the signal is 0.01m.

Figure 9 illustrates theoretical frequency response of the system with drives in position mode using pre-stressed cables in comparison to the original system with no cables.

4.1.2 Trajectory tracking

Trajectory tracking capabilities with C^1 continuous input is presented. Figure 10 shows the TCP of the system under some position changes.

The tracking error is significantly low and at the each curve change end there is a impulse because of non-smooth curve second time derivative.

4.2 Effect of cables with drives in torque control mode

Full derived model of experimental stand with described control strategy is used. The control law (33) is extended

Fig. 8 Model with auxiliary structure drives in position control mode

Fig. 9 Frequency response of beam tip position and its desired position, auxiliary structure drives are in position control mode
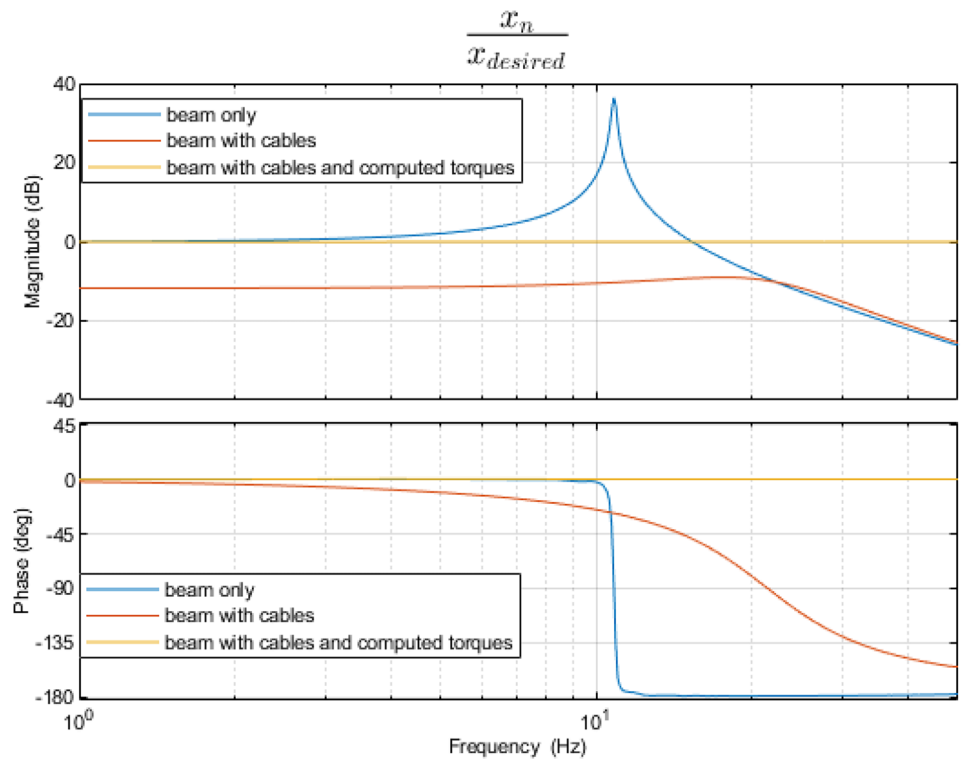

Fig. 10 Trajectory tracking with small amplitude. TCP behaviour is on top, tracking error is on the bottom. Drives are in position control mode
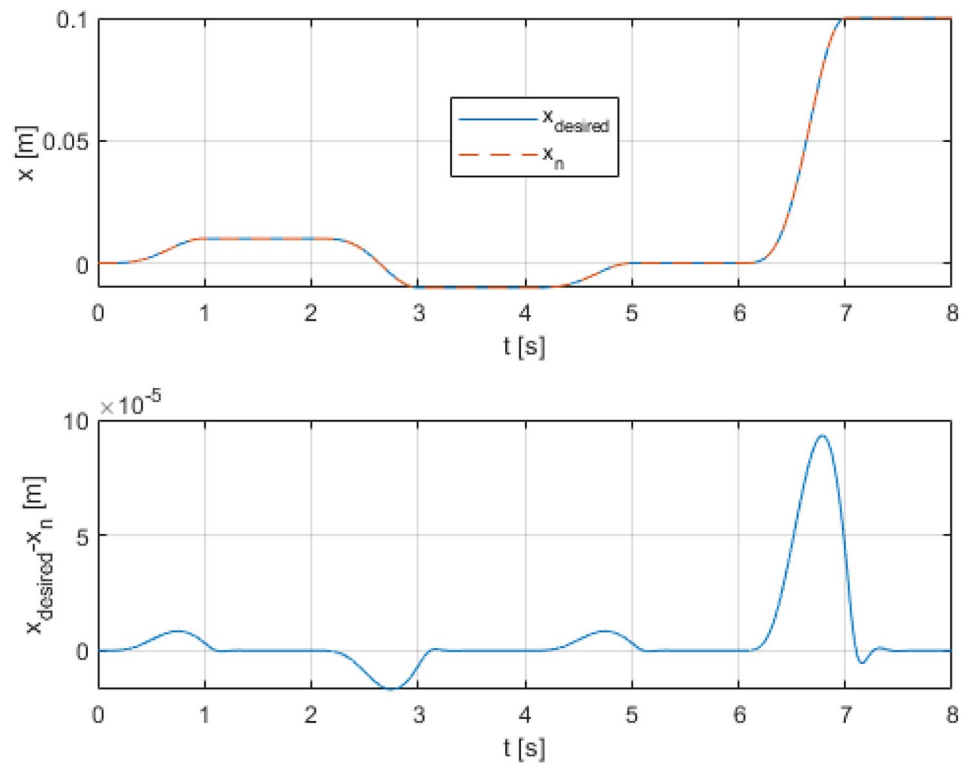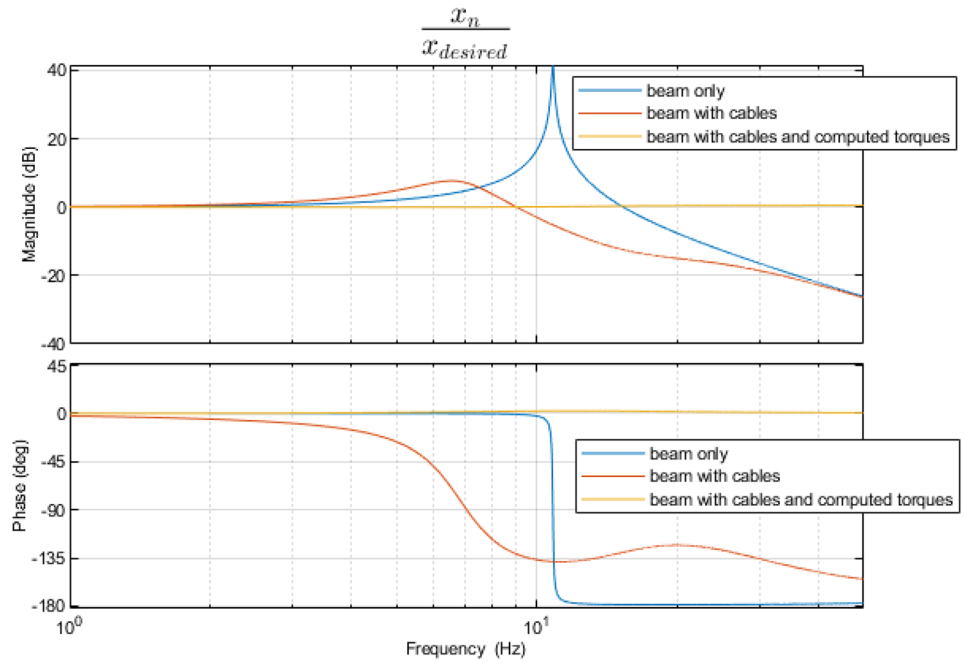
Fig. 11 Frequency response of beam tip position and its desired position, drives are in torque control mode

with I part to remove the residual control error at beam tip position (TCP point), (44). The I part gain K_{I2} equals 10^4.

$$\ddot{\mathbf{e}} + K_{d2}\dot{\mathbf{e}} + K_{p2}\mathbf{e} + K_{I2} \int \mathbf{e} = 0 \qquad (44)$$

4.2.1 Frequency response

The procedure for obtaining the frequency response of the nonlinear system with drives in torque control mode follows

Fig. 12 Trajectory tracking with small amplitude. TCP behaviour is on top, tracking error is on the bottom. Drives are in torque control mode
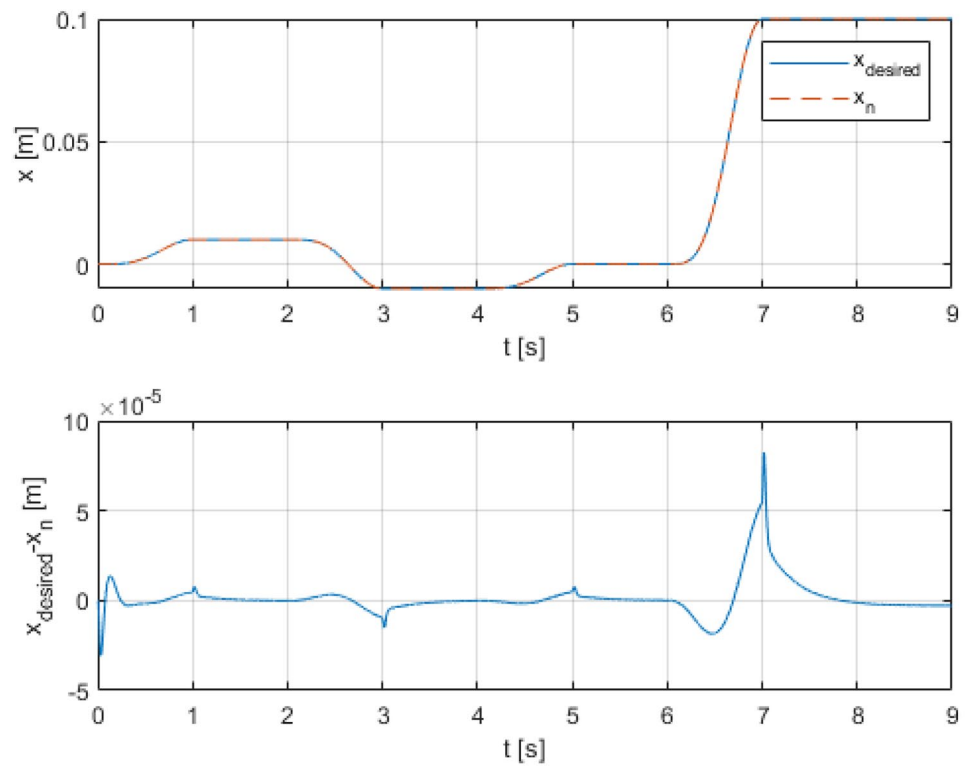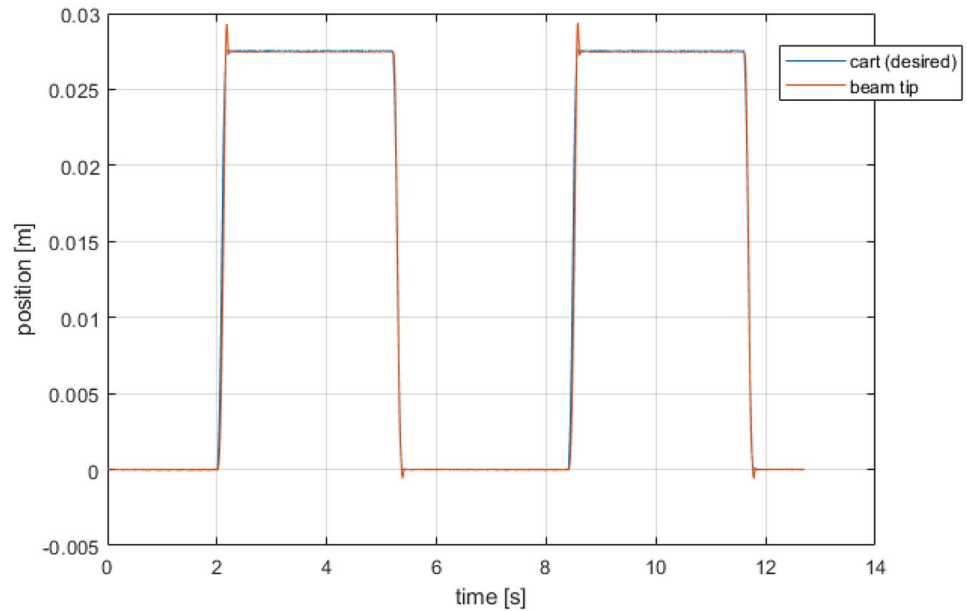
Fig. 13 Preliminary measurement, cart position measurement is a reference

on the previous case. The excitation has the same frequency and amplitude.

The frequency response of three variants (beam, beam supported with prestressed cables and beam with cables under control) is shown in Fig. 11.

4.2.2 Trajectory tracking

There is presented trajectory tracking, with same input as in previous case. Figure 12 shows the beam tip movement as well as the cart position as a desired motion.

The tracking error has satisfactory behaviour and at the each curve change end there is a impulse because of non-smooth curve second time derivative. In comparison with the drives in position control mode the tracking error is lower and behaviour is more converging, approximately $5 \cdot 10^{-5} m$ is peak value.

5 Preliminary experimental results

There is performed preliminary experimental measurement. The demonstrator on Fig. 1 consists of the cart mounted to linear axis Rexroth with the electric drive Kollmorgen 6SM 57M-3.000-S3-1325. There is mounted on a cart a beam equipped at the tip with the cables. The cables are actuated with electric drives Kollmorgen D062M-92-9310-010. The cart and beam tip horizontal positions are measured by lasertracker Leica AT960-MR and Leica AT901-B respectively. Whole system is managed by real-time control system Beckhoff AX5911 TwinCAT3 based on bus EtherCAT. The

sampling frequency is $1kHz$. The whole experiment is laboratory implementation of the demonstrator with its limitations. The practical implementation may vary significantly. The system reacts to almost step response at cart position and beam tip is controlled using cable structure.

The comparison of beam tip position with desired movement of cart is on Fig. 13. Except the peaks after the extreme step, the control error has magnitude lower than $10^{-4} m$. Further improvements to the experiment implementation are under development.

6 Conclusions

A fundamental model of the machine tool quill and supporting structure was created. The component parameters are obtained by experimental identification. Control algorithm based on the computed torques method with a PD controller was created. As part of the procedure, the cable pre-tension is included. The resulting controlled nonlinear system model was subjected to frequency analysis and subsequent trajectory tracking was evaluated.

The obtained results can be summarized as follows:

- The machine tools with a large workspace and long and heavy movable parts main properties are represented by given experimental setup
- The experimental setup is extended by auxiliary cable structure with actuators, and it creates the so-called mechatronic stiffness

- Auxiliary structure with cables can be easily modified and the original machine tool workspace is not negatively affected
- Machine tool utility properties are significantly improved
- The improvement is based on the possibility of direct control at the site of the technological process
- The controlled system frequency response shows the balanced behaviour
- Applied mechatronic stiffness concept significantly increases trajectory tracking precision
- Two different servo-drive control strategies were performed
- Preliminary experimental results show the promising behaviour of the controlled structure, and further improvements to the experiment implementation are under development

The results obtained from the simulation experiment show a significant improvement in the utility properties of the machine. Mentioned improvement is based on the possibility of direct control at the site of the technological process. This solution requires some space for the cable installation and appropriate control and power technology implementation. The structure is extended by other elements and actuators, which are however commonly used. The actual basic structure can be lightened while maintaining the existing properties with regard to the application of mechatronic stiffness or the mechatronic solution will improve the dynamic properties of the existing system. Integration into existing control systems is possible.

Availability of data and material Not applicable.

Code availability Not applicable.

Declarations

Consent to participate Not applicable.

Consent for publication Not applicable.

Competing interests The authors declare no competing interests.

References

1. Necas M, Valasek M (2019) Experimental verification of mechatronic stiffness. Proceedings - 25th Danubia-Adria Symposium on Advances in Experimental Mechanics, DAS 2008 183–184
2. Necas M, Valasek M (2009) Mechatronic stiffness of MIMO compliant branched structures by active control from auxiliary structure. Recent Advances in Mechatronics 2008-2009 167–172. https://doi.org/10.1007/978-3-642-05022-0_29
3. Ansoategui I, Campa FJ, Lopez C, Diez M (2017) Influence of the machine tool compliance on the dynamic performance of the servo drives. Int J Adv Manuf Technol 90(9–12):2849–2861. https://doi.org/10.1007/s00170-016-9616-y
4. Brenner F, Lechler A, Verl A (2021) Acceleration-based disturbance compensation for elastic rack-and-pinion drives. Prod Eng Res Devel. https://doi.org/10.1007/s11740-021-01068-w
5. Beudaert X, Franco O, Erkorkmaz K, Zatarain M (2020) Feed drive control tuning considering machine dynamics and chatter stability. CIRP Ann 69(1):345–348. https://doi.org/10.1016/j.cirp.2020.04.054
6. Wang C, Zhang X, Liu Y, Cao H, Chen X (2018) Stiffness variation method for milling chatter suppression via piezoelectric stack actuators. Int J Mach Tools Manuf 124:53–66. https://doi.org/10.1016/j.ijmachtools.2017.10.002
7. Denkena B, Bergmann B, Teige C (2018) Frictionally damped tool holder for long projection cutting tools. Prod Eng Res Devel 12(6):715–722. https://doi.org/10.1007/s11740-018-0847-7
8. Brecher C, Manoharan D, Ladra U, Köpken H-G (2010) Chatter suppression with an active workpiece holder. Prod Eng Res Devel 4(2–3):239–245. https://doi.org/10.1007/s11740-009-0204-y
9. Li L, Sun B, Hua H (2019) Nonlinear system modeling and damping implementation of a boring bar. Int J Adv Manuf Technol 104(1–4):921–930. https://doi.org/10.1007/s00170-019-03907-8
10. Valášek M, Olgac N, Neusser Z (2019) Real-time tunable single-degree of freedom, multiple-frequency vibration absorber. Mech Syst Signal Process 133:106244. https://doi.org/10.1016/j.ymssp.2019.07.025
11. Valasek M, Olgac N, Neusser Z (2019) Exploring operational frequency ranges for actively-tuned single-mass, multiple-frequency vibration absorber. 2019 5th Indian Control Conference, ICC 2019 - Proceedings, pp 448–453. https://doi.org/10.1109/INDIANCC.2019.8715571
12. Šika Z, Vyhlídal T, Neusser Z (2021) Two-dimensional delayed resonator for entire vibration absorption. J Sound Vib 500:116010. https://doi.org/10.1016/j.jsv.2021.116010
13. Vyhlídal T, Michiels W, Neusser Z, Bušek J, Šika Z (2022) Analysis and optimized design of an actively controlled two-dimensional delayed resonator. Mech Syst Signal Process. https://doi.org/10.1016/j.ymssp.2022.109195
14. Li B, Hong J, Liu Z (2014) Stiffness design of machine tool structures by a biologically inspired topology optimization method. Int J Mach Tools Manuf 84:33–44. https://doi.org/10.1016/j.ijmachtools.2014.03.005
15. Dounar S, Lakimovitch A, Jakubowski A (2021) Finite element analysis of the dynamically created portal in the huge machine tool of "travelling column" type. Scientific Journals of the Maritime University of Szczecin-Zeszyty Naukowe Akademii Morskiej w Szczecinie 65(137):29–37. https://doi.org/10.17402/458
16. Möhring H-C et al (2020) Intelligent lightweight structures for hybrid machine tools. Prod Eng Res Devel 14(5–6):583–600. https://doi.org/10.1007/s11740-020-00988-3
17. Caro S, Dumas C, Garnier S, Furet B (2013) Workpiece placement optimization for machining operations with a KUKA KR270-2 robot. 2013 IEEE International Conference on Robotics and

Automation. IEEE, pp 2921–2926. https://doi.org/10.1109/ICRA.2013.6630982

18. Furtado LFF, Villani E, Trabasso LG, Sutério R (2017) A method to improve the use of 6-dof robots as machine tools. Int J Adv Manuf Technol 92(5–8):2487–2502. https://doi.org/10.1007/s00170-017-0336-8

19. Roesch O, Zaeh MF (2014) Fuzzy controller for the compensation of path deviations during robotic milling operations. 2014 IEEE International Conference on Mechatronics and Automation. IEEE, pp 192–197. https://doi.org/10.1109/ICMA.2014.6885694

20. de Wilde WP (2006) Conceptual design of lightweight structures: the role of morphological indicators and the structural index. High Performance Structures and Materials III. WIT Press, Southampton, UK, pp 3–12. https://doi.org/10.2495/HPSM06001

21. Yongxin LI, Baosu G, Fenghe W, Kai X, Xiaoke X (2017) Lightweight design method for complex structures considering stiffness reliability. Proceedings of the 2nd International Conference on Robotics, Control and Automation - ICRCA '17. ACM Press, New York, New York, USA, pp 45–49. https://doi.org/10.1145/3141166.3141179

22. Liu T et al (2019) Improved mechanical design and simplified motion planning of hybrid active and passive cable-driven segmented manipulator with coupled motion. 2019 IEEE/RSJ International Conference on Intelligent Robots and Systems (IROS). IEEE, pp 5978–5983. https://doi.org/10.1109/IROS40897.2019.8968610

23. Jalali MH, Rideout G (2019) Analytical and experimental investigation of cable-beam system dynamics. J Vib Control 25(19–20):2678–2691. https://doi.org/10.1177/1077546319867171

24. Huang Y-X, Tian H, Zhao Y (2016) Effects of cable on the dynamics of a cantilever beam with tip mass. Shock Vib 2016:1–10. https://doi.org/10.1155/2016/7698729

25. Tang L, Gouttefarde M, Sun H, Yin L, Zhou C (2021) Dynamic modelling and vibration suppression of a single-link flexible manipulator with two cables. Mech Mach Theory 162:104347. https://doi.org/10.1016/j.mechmachtheory.2021.104347

26. Holland DB, Virgin LN, Plaut RH (2008) Large deflections and vibration of a tapered cantilever pulled at its tip by a cable. J Sound Vib 310(1–2):433–441. https://doi.org/10.1016/j.jsv.2007.06.075

27. Sohn JW, Han YM, Choi SB, Lee YS, Han MS (2009) Vibration and position tracking control of a flexible beam using SMA wire actuators. J Vib Control 15(2):263–281. https://doi.org/10.1177/1077546308094251

28. Polach P, Hajžman M, Bulín R (2020) Modelling of dynamic behaviour of fibres and cables. Engineering Mechanics. Institute of Thermomechanics of the Czech Academy of Sciences, Prague, pp 34–43. https://doi.org/10.21495/5896-3-034

29. Polach P, Hajzman M, Dupal J (2017) Influence of the fibre damping computational model in a mechanical system on the coincidence with the experimental measurement results. Eng Rev 37(1):82–91

30. Polach P, Byrtus M, Sika Z, Hajzman M (2017) Fibre springdamper computational models in a laboratory mechanical system and validation with experimental measurement. The Interdisciplinary Journal of Discontinuity, Nonlinearity, and Complexity 6(4):513–523. https://doi.org/10.5890/DNC.2017.12.009

31. Polach P, Hajžman M, Šika Z, Červená O, Svatoš P (2014) Influence of the mass of the weight on the dynamic response of the asymmetric laboratory fibre-driven mechanical system. Appl Comput Mech 8(1):75–90

32. Xiong H, Diao X (2020) Stiffness analysis of cable-driven parallel mechanisms with cables having large sustainable strains. Proc Inst Mech Eng C J Mech Eng Sci 234(10):1959–1968. https://doi.org/10.1177/0954406220902165

33. Endo G, Horigome A, Takata A (2019) Super dragon: a 10-m-long-coupled tendon-driven articulated manipulator. IEEE Robot Autom Lett 4(2):934–941. https://doi.org/10.1109/LRA.2019.2894855

34. Wang X, Zhang Q, Shen X, Li J (2020) Noncollocated position control of tendon-sheath actuated slender manipulator. IEEE Trans Control Syst Technol 28(2):688–696. https://doi.org/10.1109/TCST.2018.2884222

35. Mardani A, Ebrahimi S (2016) Computational dynamic modeling and sequential PID controlling of a tendon-based manipulator with highly slender flexible arms. 2016 4th International Conference on Robotics and Mechatronics (ICROM). IEEE, pp 542–547. https://doi.org/10.1109/ICRoM.2016.7886800

36. Wolf S et al (2016) Variable stiffness actuators: review on design and components. IEEE/ASME Trans Mechatron 21(5):2418–2430. https://doi.org/10.1109/TMECH.2015.2501019

37. Braun D, Howard M, Vijayakumar S (2012) Optimal variable stiffness control: formulation and application to explosive movement tasks. Auton Robot 33(3):237–253. https://doi.org/10.1007/s10514-012-9302-3

38. Ayoubi Y, Laribi MA, Arsicault M, Zeghloul S (2020) Safe pHRI via the variable stiffness safety-oriented mechanism (V2SOM): simulation and experimental validations. Appl Sci 10(11):3810. https://doi.org/10.3390/app10113810

39. Geeroms J, Flynn L, Jimenez-Fabian R, Vanderborght B, Lefeber D (2018) Energetic analysis and optimization of a MACCEPA actuator in an ankle prosthesis. Auton Robot 42(1):147–158. https://doi.org/10.1007/s10514-017-9641-1

40. Dou W et al (2021) Soft robotic manipulators: designs, actuation, stiffness tuning, and sensing. Adv Mater Technol 2100018. https://doi.org/10.1002/admt.202100018

41. Halamka V et al (2021) Drive axis controller optimization of production machines based on dynamic models. Int J Adv Manuf Technol 115(4):1277–1293. https://doi.org/10.1007/s00170-021-07160-w

42. Beneš P, Valášek M, Šika Z, Zavřel J, Pelikán J (2019) Shavo control: the combination of the adjusted command shaping and feedback control for vibration suppression. Acta Mech 230(5):1891–1905. https://doi.org/10.1007/s00707-019-2363-z

43. Liu Q et al (2020) A non-delay error compensation method for dual-driving gantry-type machine tool. Processes 8(7):748. https://doi.org/10.3390/pr8070748

44. Huang Y, Liu Z, Du R, Tang H (2019) Simulation and experiments of active vibration control for ultra-long flexible manipulator under impact loads. J Vib Control 25(3):675–684. https://doi.org/10.1177/1077546318794222

45. Neusser Z, Valášek, M (2013) Control of the double inverted pendulum on a cart using the natural motion. Acta Polytechnica 53(6):883–889. https://doi.org/10.14311/AP.2013.53.0883

46. Neusser Z, Nečas M, Valášek M (2022) Control of flexible robot by harmonic functions. Appl Sci (Switzerland) 12(7). https://doi.org/10.3390/app12073604

47. Valášek M, Šika Z (2001) Evaluation of dynamic capabilities of machines and robots. Multibody SysDyn 6(2):183–202. https://doi.org/10.1023/A:1017520006170

48. Procházka F, Valášek M, Šika Z (2016) Robust sliding mode control of redundantly actuated parallel mechanisms with respect to geometric imperfections. Multibody SysDyn 36(3):221–236. https://doi.org/10.1007/s11044-015-9481-8

49. Wu J, Yu G, Gao Y, Wang L (2018) Mechatronics modeling and vibration analysis of a 2-DOF parallel manipulator in a 5-DOF hybrid machine tool. Mech Mach Theory 121:1339–1351. https://doi.org/10.1016/j.mechmachtheory.2017.10.023

50. Wu J, Song Y, Liu Z, Li G (2022) A modified similitude analysis method for the electro-mechanical performances of a parallel manipulator to solve the control period mismatch problem. Science China Technol Sci 65(3):541–552. https://doi.org/10.1007/s11431-021-1955-8

51. Wu J, Zhang B, Wang L, Yu G (2021) An iterative learning method for realizing accurate dynamic feedforward control of an industrial hybrid robot. Science China Technol Sci 64(6):1177–1188. https://doi.org/10.1007/s11431-020-1738-5

52. Gao X et al (2022) Dynamic modeling and analysis on lateral vibration of ball screw feed system. Int J Adv Manuf Technol. https://doi.org/10.1007/s00170-022-09525-1

53. Sakai Y, Tanaka T (2020) Influence of lubricant on nonlinear vibration characteristics of linear rolling guideway. Tribol Int. https://doi.org/10.1016/j.triboint.2019.106124

54. Zhao P, Huang J, Shi Y (2017) Nonlinear dynamics of the milling head drive mechanism in five-axis CNC machine tools. Int J Adv Manuf Technol 91(9–12):3195–3210. https://doi.org/10.1007/s00170-017-9989-6

55. Balachandran B, Zhao M (2000) A mechanics based model for study of dynamics of milling operations. Meccanica 35(2):89–109. https://doi.org/10.1023/A:1004887301926

56. Rusinek R, Wiercigroch M, Wahi P (2014) Modelling of frictional chatter in metal cutting. Int J Mech Sci 89:167–176. https://doi.org/10.1016/j.ijmecsci.2014.08.020

57. Huo D, Cheng K, Wardle F (2010) Design of a five-axis ultra-precision micro-milling machine-UltraMill. Part 1: holistic design approach, design considerations and specifications. Int J Adv Manuf Technol 47(9–12):867–877. https://doi.org/10.1007/s00170-009-2128-2

58. Gou N, Cheng K, Huo D (2021) Multiscale modelling and analysis for design and development of a high-precision aerostatic bearing slideway and its digital twin. Machines 9(5). https://doi.org/10.3390/machines9050085

59. Neusser, Z., Nečas, M., Pelikán, J. et al. Active vibration damping for manufacturing machines using additional cable mechanisms: conceptual design. Int J Adv Manuf Technol (2022). https://doi.org/10.1007/s00170-022-10075-9